THE JOURNAL OF BIOLOGICAL CHEMISTRY VOL. 289, NO. 44, pp. 30772–30784, October 31, 2014

Mouse Macrophages Completely Lacking Rho Subfamily GTPases (RhoA, RhoB, and RhoC) Have Severe Lamellipodial Retraction Defects, but Robust Chemotactic Navigation and Altered Motility*[S]

Received for publication, March 6, 2014, and in revised form, August 19, 2014 Published, JBC Papers in Press, September 11, 2014, DOI 10.1074/jbc.M114.563270

Volker Königs[‡], Richard Jennings[§], Thomas Vogl[¶], Markus Horsthemke[‡], Anne C. Bachg[‡], Yan Xu[‡], Kay Grobe[‖], Cord Brakebusch[**], Albrecht Schwab[‡‡], Martin Bähler[‡], Ulla G. Knaus[§], and Peter J. Hanley[‡1]

From the [‡]Institut für Molekulare Zellbiologie, Wilhelms-Universität Münster, 48149 Münster, Germany, the [§]Conway Institute, University College Dublin, Dublin, Ireland, the [¶]Institut für Immunologie, [‖]Institut für Physiologische Chemie und Pathobiochemie, and [‡‡]Institut für Physiologie II, Wilhelms-Universität Münster, 48149 Münster, Germany, and the [**]Biotech Research and Innovation Centre (BRIC), University of Copenhagen, 2200 Copenhagen, Denmark

Background: RhoA is strongly implicated in cell motility.
Results: Macrophages lacking RhoA or RhoB have mild phenotypes, whereas double mutants, which also lack RhoC, exhibit severe cytoskeletal defects, but robust chemotaxis.
Conclusion: RhoA and RhoB have overlapping functions in tail and lamellipodial membrane retraction, but are not critical for motility.
Significance: The Rho subfamily is largely redundant for "front end" functions of motility and chemotaxis.

RhoA is thought to be essential for coordination of the membrane protrusions and retractions required for immune cell motility and directed migration. Whether the subfamily of Rho (Ras homolog) GTPases (RhoA, RhoB, and RhoC) is actually required for the directed migration of primary cells is difficult to predict. Macrophages isolated from myeloid-restricted RhoA/RhoB (conditional) double knock-out (dKO) mice did not express RhoC and were essentially "pan-Rho"-deficient. Using real-time chemotaxis assays, we found that retraction of the trailing edge was dissociated from the advance of the cell body in dKO cells, which developed extremely elongated tails. Surprisingly, velocity (of the cell body) was increased, whereas chemotactic efficiency was preserved, when compared with WT macrophages. Randomly migrating RhoA/RhoB dKO macrophages exhibited multiple small protrusions and developed large "branches" due to impaired lamellipodial retraction. A mouse model of peritonitis indicated that monocyte/macrophage recruitment was, surprisingly, more rapid in RhoA/RhoB dKO mice than in WT mice. In comparison with dKO cells, the phenotypes of single RhoA- or RhoB-deficient macrophages were mild due to mutual compensation. Furthermore, genetic deletion of RhoB partially reversed the motility defect of macrophages lacking the RhoGAP (Rho GTPase-activating protein) myosin IXb (Myo9b). In conclusion, the Rho subfamily is not required for "front end" functions (motility and chemotaxis), although both RhoA and RhoB are involved in pulling up the "back end" and resorbing lamellipodial membrane protrusions. Macrophages lacking Rho proteins migrate faster *in vitro*, which, in the case of the peritoneum, translates to more rapid *in vivo* monocyte/macrophage recruitment.

Professional phagocytes of the innate immune system, neutrophils and macrophages, are recruited to sites of inflammation by gradients of chemoattractant molecules, but exactly how these cells coordinate shape changes and navigate in such gradients is unclear. Like most cells, neutrophils and macrophages move on a two-dimensional surface by generating thin membrane protrusions at the front, followed by pulling forward of the cell body and retraction of the back end (1, 2), along the lines of the motility model first delineated by Abercrombie *et al.* (3) in the early 1970s (reviewed in Ref. 4). Cells may produce more than one protrusion, but ultimately, the dominant membrane protrusion determines the direction of movement (5). Chemotaxis requires that the dominant membrane protrusion is directed toward higher concentrations of chemoattractant (6). Starting with an extracellular chemoattractant (agonist) gradient, the following basic levels of signal transduction are involved in chemotaxis: agonist gradient → G protein-coupled receptors (GPCRs)[2] → signaling cascades → Rho GTPases → effector proteins → (spatially coordinated) membrane protrusions and retractions. Thus, signaling to and from Rho GTPases, molecular switches that cycle between a GTP-bound active state and GDP-bound inactive state, is required for coordinated cytoskeletal rearrangements. Members of the Rho subfamily of small monomeric Rho GTPases, which consists of

* This work was supported by the Cells in Motion (CiM) Cluster of Excellence, the Deutsche Forschungsgemeinschaft (DFG) Grant HA 3271/3-1 (to P. J. H.), and funding from the Health Research Board and Science Foundation Ireland (to U. G. K.).
[S] This article contains supplemental Videos 1–3.
[1] To whom correspondence should be addressed. Tel.: 49-251-83-23854; Fax: 49-251-83-24723; E-mail: hanley@uni-muenster.de.

[2] The abbreviations used are: GPCR, G protein-coupled receptor; dKO, double knock-out; ROCK, Rho-associated protein kinase; EGFP, enhanced green fluorescent protein; GAP, GTPase-activating protein; GEF, guanine nucleotide exchange factor; DIC, differential interference contrast; p-MLC2, phospho-myosin light chain 2.

RhoA, RhoB, and RhoC, have emerged as key signaling components and are implicated to play central roles in cell polarization, motility, and chemotaxis (7–9).

Ultimately, cell shape changes and cell motility require, in addition to local volume changes (10), the spatial coordination of two ATP-dependent events (11–13): F-actin polymerization and motor protein-driven actomyosin contraction. Activated Rho subfamily Rho GTPases act via Rho kinases (ROCK1 and ROCK2; Rho-associated coiled-coil-containing protein kinases) to induce phosphorylation of myosin II regulatory light chains, which promotes actomyosin contraction. In addition, Rho-ROCK signaling negatively regulates cofilin via LIM motif-containing protein kinase, leading to decreased F-actin dynamics. Independent of ROCK, Rho activates the formins mDia1–3 (14–16) and other signaling pathways (17, 18). Rho signaling has been implicated in various aspects of cell motility, including retraction of the rear (2), restriction of lamellipodia to the front (19), squeezing of the nucleus through narrow passages (20), and shaping the leading edge (21, 22).

Links between GPCRs and the Rho subfamily of Rho GTPases have been identified. The $G_{12/13}$ subfamily of heterotrimeric G proteins triggers activation of RhoGEFs (Rho-specific guanine nucleotide exchange factors) (23–25), such as Lsc (human homolog, p115-RhoGEF), leukemia-associated RhoGEF, and PDZ-RhoGEF, which specifically activate the Rho subfamily. Thus, the following signaling scheme may be important for motility and chemotaxis: chemoattractant agonist → GPCRs → $G_{12/13}$ → RhoGEFs → Rho subfamily GTPases (RhoA, RhoB, and RhoC) → effectors. The $G_{q/11}$ subfamily may also contribute to RhoGEF activation via GPCRs (26, 27). Knock-out mouse models may provide valuable insight into the relative importance and physiological roles of RhoA, RhoB, and RhoC in the context of innate immune cell motility and chemotaxis. Mice with global deletion of RhoB or RhoC are viable (28, 29), and macrophages derived from the bone marrow of $RhoB^{-/-}$ mice were shown to migrate faster on fibronectin, but slower on an uncoated glass surface, when compared with wild-type cells (30). RhoC has been implicated in cancer cell migration (31), whereas RhoC deficiency has been reported to have no effect on the motility of immune cells (29). In contrast to RhoB and RhoC, global deletion of RhoA in mice is lethal (32). Deletion of RhoA in mouse embryonic fibroblasts impaired mitosis (33), whereas deletion of RhoA in keratinocytes impaired directed migration, which could not be explained by disruption of ROCK signaling (34).

Here we used myeloid-restricted RhoA knock-out mice ($RhoA^{fl/fl}$/LysM-Cre), $RhoB^{-/-}$ and RhoA/RhoB double knock-out mice, as well as $Myo9b^{-/-}$ and Myo9b/RhoB double knock-out mice, to elucidate the roles of the Rho subfamily of GTPases, and their regulation, in cell polarization, motility, and chemotactic navigation, using macrophages as model cells.

EXPERIMENTAL PROCEDURES

Mice—Myeloid-restricted *RhoA* (ras homolog gene family, member A; Mouse Genome Informatics (MGI): 1096342) knock-out mice were generated by crossing floxed RhoA (34) and LysM-Cre (35) mice. These mice were further crossed with *RhoB* (ras homolog gene family, member A; MGI: 107949) knock-out mice (28) to generate RhoA (myeloid-restricted)/RhoB double knock-out mice. LysM-EGFP mice (36) were provided by Stefan Butz (Max-Planck-Institute, Münster, Germany). Myo9b/RhoB double knock-out (dKO) mice were generated by crossing *Myo9b* (myosin IXb; MGI: 106624) knock-out (1) and $RhoB^{-/-}$ mice. Mice were bred in specific pathogen-free conditions and used in accordance with local animal experimentation guidelines. All procedures were approved by the respective University of Münster and University College Dublin animal care and use committees.

Mouse Peritonitis Model—Female mice (8–12 weeks) were injected with 2 ml of PBS containing 4% thioglycollate. After 48 h, the mice were sacrificed by cervical dislocation and peritoneal cavity cells were harvested by peritoneal lavage. The cells were stained with allophycocyanin-conjugated anti-F4/80 antibodies (clone BM8; eBioscience) in cytometry buffer (PBS supplemented with 5% fetal calf serum and 0.05% NaN_3) for 30 min on ice. Cells were pelleted by centrifugation (400 × *g* for 4 min) at 4 °C and washed three times. Fluorescence of allophycocyanin-labeled F4/80 was determined using a BD Accuri C6 flow cytometer.

Antibodies—Resident peritoneal macrophages were purified by cell sorting using rat anti-mouse F4/80 antibodies conjugated to Alexa Fluor 488 (5:200, MCA497A488, AbD Serotec, Germany). Flow cytometry of LysM-EGFP peritoneal cells was performed using rat anti-mouse F4/80 antibodies conjugated to phycoerythrin (5:200, MCA497PET, AbD Serotec). The following antibodies (diluted 1:500) from Santa Cruz Biotechnology (Heidelberg, Germany) were used for Western blot analyses: mouse monoclonal anti-RhoA (26C4 (sc-418)), rabbit polyclonal anti-RhoB (119 (sc-180)), and goat polyclonal anti-RhoC (K-12 (sc-26480) or C-16 (sc-12116)). Lysates from HEK293T cells expressing mouse RhoC (sc-123119, Santa Cruz Biotechnology) were used as positive control. Myosin light chain 2 (also known as myosin regulatory light chain) phosphorylated at serine 19 was detected using rabbit polyclonal antibodies from Cell Signaling Technology (catalog number 3671). Mouse monoclonal anti-β-actin antibodies (A1978, Sigma-Aldrich, Munich, Germany), diluted 1:2000, were used to control loading in Western blot analyses.

Isolation and Handling of Resident Peritoneal Macrophages—Mice were killed by an overdose of isoflurane in air, and the peritoneal cavity was lavaged via a 24-gauge plastic catheter (B. Braun, Melsungen, Germany) using 2 × 4.5 ml of ice-cold Hanks' balanced salt solution without Ca^{2+} or Mg^{2+} (PAA Laboratories, Pasching, Austria). After centrifugation (360 × *g* for 5 min), cells were resuspended in RPMI 1640 medium containing 2 g/liter bicarbonate (Biochrom AG, Berlin, Germany) and supplemented with 10% heat-inactivated FCS, 100 units/ml penicillin, and 100 μg/ml streptomycin (pH 7.4). The cells were seeded into fibronectin-coated μ-slide I chambers or μ-slide chemotaxis chambers (Ibidi, Martinsried, Germany) and placed in a humidified incubator (37 °C, 5% CO_2). Experiments were performed on the stage of an inverted microscope (AxioVision) equipped with a temperature-controlled incubator (incubator XL S, Zeiss) using the same complete medium as above, except that bicarbonate buffer was replaced by 20 mM Hepes (pH 7.4).

Generation of Bone Marrow-derived Macrophages—After euthanasia, the mid-diaphysis of hind leg femurs was fractured using a surgical scalpel blade, and bone marrow cells were flushed out with 5 ml of RPMI 1640 Hepes medium per bone fragment. After centrifugation (300 × *g* for 11 min) at room temperature, the supernatant was removed, and 1 ml of lysis buffer (155 mM NH_4Cl, 10 mM $KHCO_3$, and 0.1 mM EDTA; pH 7.4) was added for 5 min. The suspension was centrifuged at 300 × *g* for 10 min, and the supernatant was discarded. Next, the cells were washed once with 20 ml of RPMI 1640 Hepes medium, centrifuged (300 × *g* for 11 min), and resuspended in 30 ml of RPMI 1640 bicarbonate medium containing 2% gentamycin, 1% kanamycin, 1% nonessential amino acids (100× concentrate), 10% fetal calf serum ,and 15 ng/ml recombinant mouse M-CSF (R&D systems). The suspension was incubated (37 °C, 5% CO_2) in Teflon bags (PermaLife PL30, OriGen Biomed Europe, Sweden) for 6 days.

Two-dimensional Chemotaxis Assays—Cells obtained by peritoneal lavage of a single mouse were resuspended in 200–225 μl of medium, and 8 μl of the suspension was seeded into the narrow (1000 × 2000 × 70-μm) channel of an uncoated (IbiTreat) μ-slide chemotaxis chamber (Ibidi). The narrow channel (observation area) connects two 40-μl reservoirs. After 3 h, the chemotaxis chamber was filled with RPMI 1640 (bicarbonate) medium containing 10% FCS and antibiotics.

Prior to performing assays, the chemotaxis chamber was slowly washed with bicarbonate-free medium. Next, 15 μl of medium containing 0.003% Patent Blue V (blue dye) was drawn into one of the reservoirs either without (control) or with chemoattractant (C5a). The final concentration of C5a was 20 nM. The observation area was imaged by phase-contrast microscopy via a 10×/0.3 objective. The blue dye served as a visual indicator of gradient formation and does not affect cell migration. Images were captured every 2 min for 14 h, and cell migration tracks between 6 and 12 h were analyzed with ImageJ (National Institutes of Health) using a manual tracking plugin and the chemotaxis and migration tool from Ibidi. Twenty-five randomly selected cells were manually tracked in each chemotaxis experiment.

DIC Time-lapse Imaging—μ-Slide I chambers and chemotaxis μ-slides were placed on the stage of an inverted semimotorized Zeiss AxioObserver microscope controlled by AxioVision software. The microscope was fitted with a temperature-controlled stage incubator (Zeiss, Jena, Germany), and the temperature was maintained at 37 °C. Cells were imaged via a 63×/1.4 oil immersion objective, and differential interference contrast (DIC) images were captured every 15 s by an AxioCam MRm camera (Zeiss).

Spinning Disk Confocal Microscopy—Three-dimensional images of living macrophages were obtained using an UltraVIEW Vox three-dimensional live cell imaging system (PerkinElmer, Rodgau, Germany) coupled to a Nikon Eclipse Ti inverse microscope. The system incorporated a Yokogawa (Tokyo, Japan) CSU-X1 spinning disk scanner, a Hamamatsu (Tokyo, Japan) C9100-50 EM-CCD camera (1000 × 1000 pixels), and Volocity software. Cells were imaged via a Nikon 60× (NA 1.49) oil immersion objective lens, and the temperature was maintained at 37 °C using an Okolab all-in-one stage incubator (Okolab, Ottaviano, Italy). Z-stacks of macrophages labeled with Alexa Fluor 488- (Invitrogen) or Alexa Fluor 594-conjugated (BioLegend, Fell, Germany; catalog number 123140) anti-F4/80 antibodies were obtained using 0.5-μm steps.

Flow Cytometry and Cell Sorting—Cell sorting and cell analyses were performed using a BD FACSAria II (or FACSAria III) cell sorter (BD Biosciences). Alternatively, cell analysis was performed using a FACSCalibur flow cytometer, and data were analyzed using FlowJo software (Tree Star, Ashland, OR).

Superresolution Structured Illumination Microscopy—Macrophages were fixed by incubation with 4% paraformaldehyde in PBS at 37 °C for 18 min and permeabilized by incubation with 0.1% Triton X-100 in PBS at room temperature for 25 min. F-actin was stained with Alexa Fluor 488-conjugated phalloidin (Invitrogen, Darmstadt, Germany) and imaged, via a 63× (NA 1.4) oil immersion objective lens, by superresolution structured illumination microscopy using an Elyra S.1 microscope system (Carl Zeiss MicroImaging, Jena, Germany).

Western Blot Analysis—Macrophages were lysed in buffer containing 50 mM Tris-HCl (pH 7.4), 100 mM NaCl, 2 mM $MgCl_2$, 1 mM dithiothreitol, 1% Nonidet P-40, 10% glycerol, 5 mM NaF, 1 mM Na_3VO_4 (sodium orthovanadate), and the protease inhibitors leupeptin, aprotinin, and Pefabloc (each at 10 μg/ml). Proteins were separated by 15% SDS-PAGE and transferred onto polyvinylidene difluoride membranes (Roche Applied Science, Mannheim, Germany). Membranes were blocked for 1 h at room temperature in TBS containing 5% bovine serum albumin and 0.1% Tween 20 followed by overnight incubation (4 °C) with primary antibodies. For detection, horseradish peroxidase-conjugated secondary antibodies (Dianova, Hamburg, Germany) were used in combination with SuperSignal West Pico chemiluminescence substrate (Perbio, Bonn, Germany).

Statistics—Normality and homoscedasticity were tested using the Shapiro-Wilk and Levene tests, respectively. A one-way analysis of variance was used to test for statistical differences at the 0.05 level of significance. When the assumed conditions of normality and homogeneity of variance were not fulfilled, as in most cases, we used the nonparametric Kruskal-Wallis one-way analysis of variance on ranks (at the 0.05 level of significance). Post hoc multiple comparisons were made using Dunn's method. Statistical analyses were performed using SigmaPlot (version 12) software (Systat Software, Erkrath, Germany), and data are presented as means ± S.E.

RESULTS

RhoA and RhoB, but Not RhoC, Are Expressed in Mouse Macrophages—Mouse macrophages move by generating a membrane protrusion in the direction of movement (Fig. 1*A*). As shown in the time-lapse sequence (Fig. 1*A*), cells may produce more than one protrusion, typically by splitting an existing one, but ultimately one protrusion will become dominant and determine the direction of movement, whereas secondary protrusions are retracted. We started out with a working model of a polarized and migrating macrophage (Fig. 1*B*) in which RhoA is active at the back and sides, whereas it is inhibited by the RhoGAP (Rho-specific GTPase-activating protein) Myo9b at

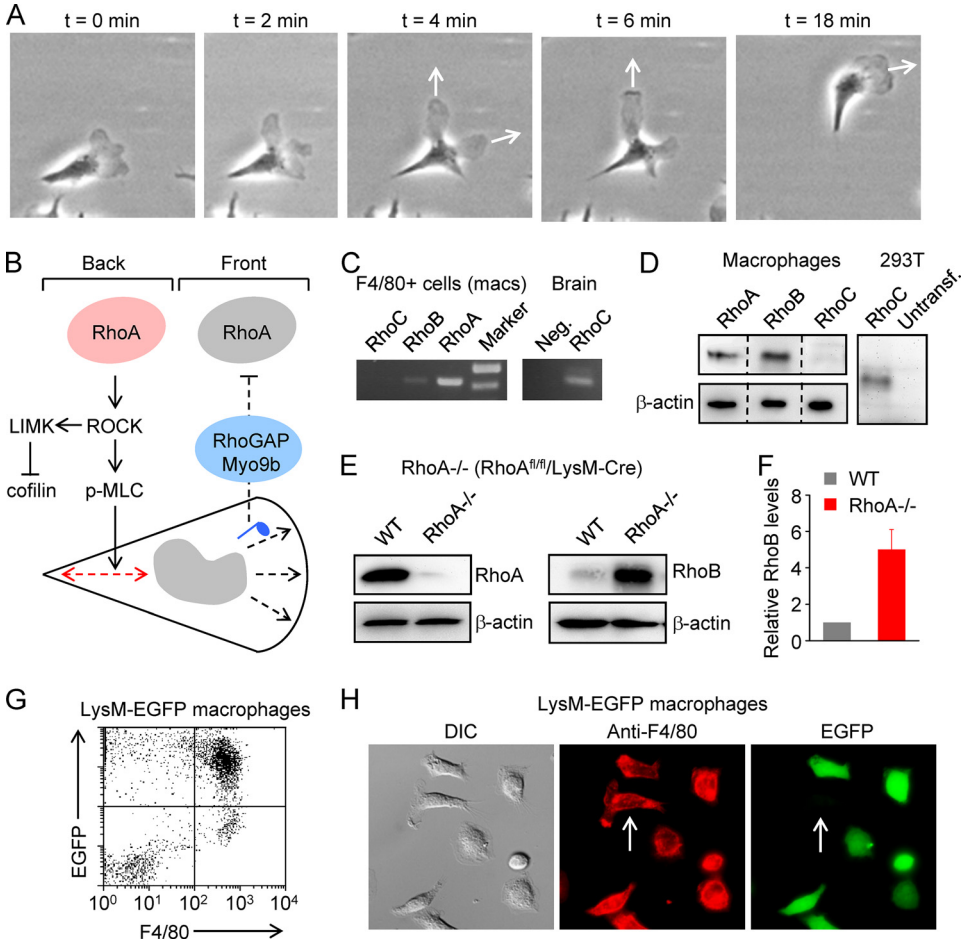

FIGURE 1. **Working model and conditional deletion of RhoA in macrophages.** *A*, time-lapse phase-contrast images (100 × 100 μm, except for $t = 2$ min) of a migrating mouse resident peritoneal macrophage. *White arrows* indicate the projected direction of prominent membrane protrusions. *B*, schematic working model of spatially coordinated Rho signaling in a migrating macrophage. *C*, gene analysis by RT-PCR. Peritoneal F4/80$^+$ cells (macrophages) purified by cell sorting express mRNA for RhoA and RhoB, but not RhoC. *D*, Western blot analysis. RhoA and RhoB, but not RhoC, protein could be detected in macrophages. Note that primary antibodies against RhoA, RhoB, or RhoC were applied after cutting the membrane into strips. Lysates from HEK293T cells expressing mouse RhoC were used as positive control. *E*, Western blot analysis of RhoA and RhoB in macrophages derived from conditional RhoA knock-out mice, obtained by crossing floxed RhoA (RhoA$^{fl/fl}$) and LysM-Cre mice. A very weak RhoA signal could be detected in macrophages isolated from RhoA$^{fl/fl}$/LysM-Cre mice, and RhoB levels were markedly increased in these cells. *F*, high expression levels of RhoB in RhoA$^{-/-}$ macrophages relative to WT cells ($n = 5$). *Error bars* indicate means ± S.E. *G*, flow cytometry analysis of macrophages isolated from LysM-EGFP mice and labeled with phycoerythrin-conjugated anti-F4/80 antibodies. *H*, DIC and fluorescence images of macrophages isolated from a transgenic mouse expressing EGFP (rather than Cre) under the control of the M lysozyme gene. Note that one of the F4/80$^+$ cells (indicated by a *white arrow*) does not appear to express EGFP. Images are 100 × 100 μm.

the front (1). RT-PCR analyses showed that F4/80$^+$ cells (macrophages) express mRNA for RhoA and RhoB, but not RhoC (Fig. 1*C*). Consistent with these findings, RhoA and RhoB, but not RhoC, protein could be detected by Western blot (Fig. 1*D*). Lysates from HEK293T cells expressing mouse RhoC were used as positive control. Next, we investigated the effects of conditional RhoA deletion on cell morphology, motility, and chemotactic navigation.

RhoA-deficient Macrophages—Mice with conditional knock-out of RhoA in myeloid cells were generated by crossing floxed RhoA (RhoA$^{fl/fl}$) mice (34) with LysM-Cre mice (35), in which Cre (Cre recombinase) is expressed under the control of the myeloid-restricted M lysozyme gene. Western blot analyses indicated almost complete loss of RhoA in macrophages derived from RhoA$^{fl/fl}$/LysM-Cre mice (Fig. 1*E*). Notably, RhoB levels were markedly increased (by a factor of ~5) in RhoA-deficient macrophages (Fig. 1, *E* and *F*). Up-regulation of RhoB levels has been observed in RhoA-deficient keratinocytes (34) and may be an indicator that RhoB functionally compensates for RhoA deficiency.

We speculated that the weak RhoA protein detection in macrophages from myeloid-restricted conditional RhoA knock-out (RhoA$^{fl/fl}$/LysM-Cre) mice may be due to lack of Cre expression in a subpopulation of cells. Therefore, we analyzed enhanced green fluorescent protein (EGFP) expression in transgenic mice expressing EGFP under the control of the M lysozyme gene (35). FACS analysis revealed that >90% of resident F4/80$^+$ cells isolated from the peritoneum were EGFP-positive (Fig. 1*G*). About 10–15% of mouse peritoneal macrophages are F4/80-negative, which explains the detection of F4/80^{lo}EGFP^{hi} cells. Consistent with the FACS analysis, we found that EGFP fluorescence could be detected in 91 ± 0.9% ($n = 5$; 112 cells) of F4/80$^+$ peritoneal macrophages plated on Ibidi fibronectin-coated μ-slide I chambers (Fig. 1*H*). Thus, in accord with Clausen *et al.* (35), Cre recombinase is expected to be expressed in >90% of individual macrophages isolated from

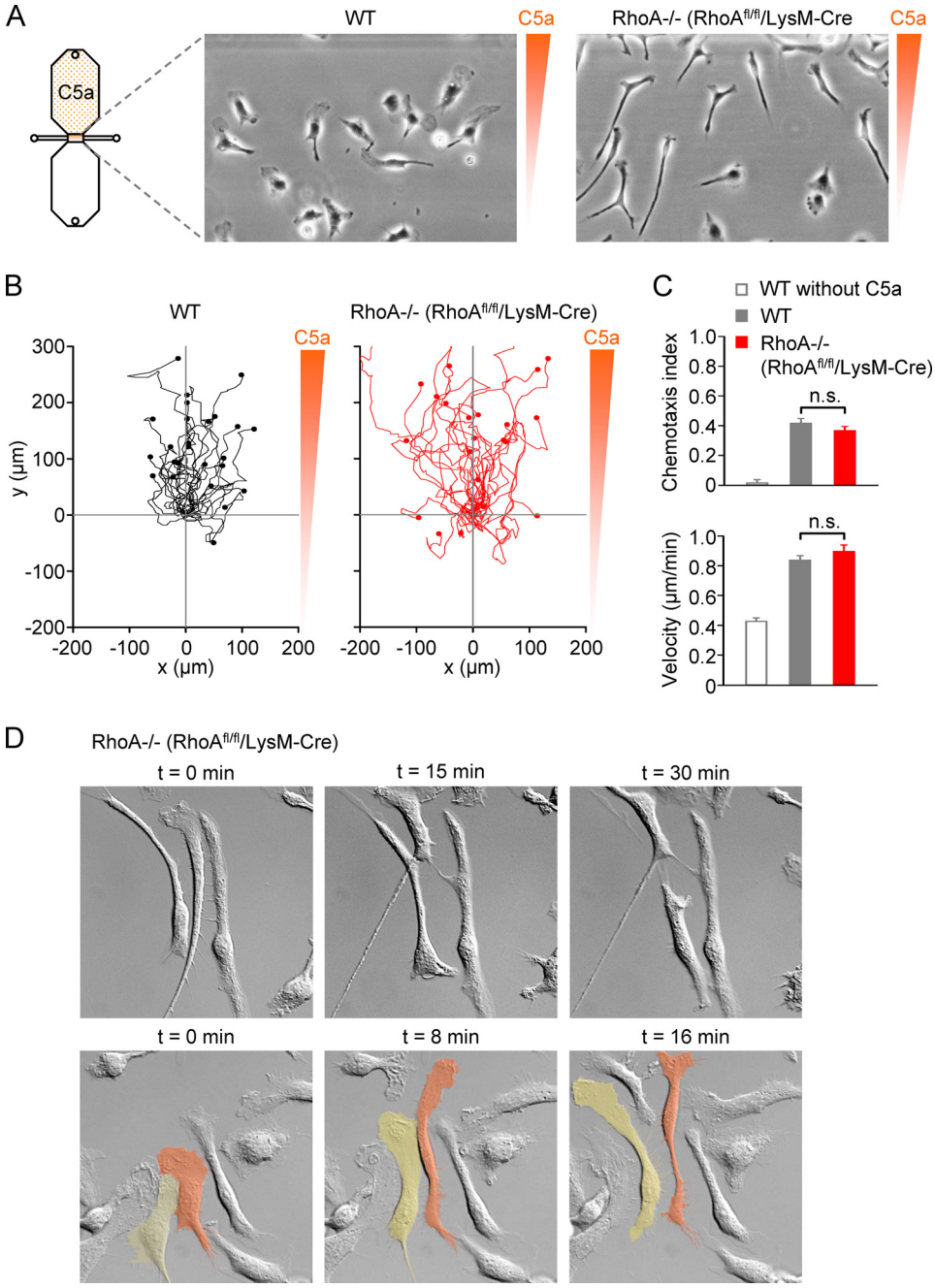

FIGURE 2. **Phenotype and chemotactic behavior of RhoA-deficient macrophages.** *A*, schematic diagram of a chemotaxis μ-slide and 200 × 300-μm snapshots of WT and RhoA-deficient (RhoA$^{fl/fl}$/LysM-Cre) macrophages in a chemotactic complement component C5a gradient. *B*, migration plots of WT and RhoA-deficient (RhoA$^{fl/fl}$/LysM-Cre) macrophages in a C5a gradient. *C*, summary plots of chemotactic efficiency (chemotaxis index) and mean velocity. The summary bar labeled *WT without C5a* refers to WT cells migrating in the absence of chemoattractant. *Error bars* indicate means ± S.E. *n.s.*, not significant. *D*, high resolution DIC images of spontaneously migrating RhoA-deficient macrophages. Images are 100 × 100 μm. In the *lower panel*, two migrating cells have been pseudocolored to distinguish them from neighboring cells.

LysM-Cre mice. This implies that the weak detection of RhoA protein in macrophages isolated from RhoA$^{fl/fl}$/LysM-Cre mice (Fig. 1*E*) can be attributed to the presence of Cre recombinase-negative cells.

Impaired Tail Retraction, but Preserved Velocity and Chemotactic Efficiency, in RhoA-deficient Macrophages—To investigate whether RhoA is required for motility and chemotactic navigation, and especially tail retraction, as indicated in our working model (Fig. 1*B*), we performed real-time chemotaxis assays (1). Peritoneal macrophages were seeded into the narrow channel (observation area) of a μ-slide chemotaxis chamber, and complement component C5a was added to one of the two 40-μl reservoirs to generate a chemotactic gradient (Fig. 2*A*). Snapshots of wild-type (WT) and RhoA$^{-/-}$ (RhoA$^{fl/fl}$/LysM-Cre) macrophages migrating in a chemotactic complement component C5a gradient are shown in Fig. 2*A*. Note that the lamellipodia of most wild-type macrophages are directed toward the source of chemoattractant. Migration plots of individual wild-type and RhoA$^{-/-}$ (RhoA$^{fl/fl}$/LysM-Cre) macrophages, obtained by tracking 25 randomly selected cells

between 6 and 12 h after the addition of complement component C5a to one of the reservoirs (final concentration, 20 nM), are shown in Fig. 2*B*. In the absence of chemoattractant, WT macrophages showed no preferential direction of movement, as expected, and mean migration velocity was ~0.4 μm/min (Fig. 2*C*). In a chemotactic C5a gradient, wild-type and RhoA$^{-/-}$ (RhoA$^{fl/fl}$/LysM-Cre) macrophages had a mean chemotaxis index of ~0.4 and a mean migration velocity of ~0.8 μm/min (Fig. 2*C*). The chemotaxis index, also known as the *y*-forward migration index, is calculated by dividing the displacement parallel to the *y* axis (chemoattractant gradient axis) by the total path length (traveled by the cell), and it varies between −1 and +1. Cells were tracked by manually clicking on the cell body. Taken together, the WT *versus* RhoA$^{-/-}$ chemotaxis assays indicated that RhoA has no significant effect on the velocity and chemotactic efficiency of macrophages. However, RhoA deficiency affected cell morphology.

The most notable feature of RhoA$^{-/-}$ (RhoA$^{fl/fl}$/LysM-Cre) macrophages in a chemotactic gradient was the development of elongated trailing ends. Although this phenotype of moderately impaired tail retraction can be identified in snapshots of RhoA$^{-/-}$ (RhoA$^{fl/fl}$/LysM-Cre) macrophages, time-lapse imaging (Fig. 2*D*) revealed that individual migrating cells alternately elongated and shortened. That is, there was an increased tendency for the trailing end of a migrating RhoA$^{-/-}$ cell to lag temporarily behind the cell body.

Striking Phenotype of "pan-Rho" Knock-out (RhoA$^{fl/fl}$/LysM-Cre/RhoB$^{-/-}$) Macrophages—The greatly increased RhoB protein levels in RhoA$^{-/-}$ macrophages, as well as the moderate elongated phenotype of RhoA$^{-/-}$ cells, suggested that RhoB may compensate for loss of RhoA. Conversely, we found that RhoA protein levels were increased in RhoB$^{-/-}$ macrophages (Fig. 3, *A* and *B*), indicating mutual regulation of RhoA and RhoB expression. We reasoned that RhoA and RhoB take part in common cellular functions associated with cell shape control and motility. To explore this possibility, we produced macrophages lacking both RhoA and RhoB by crossing RhoA$^{fl/fl}$/LysM-Cre and RhoB$^{-/-}$ mice. Western blot analysis confirmed that RhoA/RhoB dKO macrophages lacked RhoA and RhoB (Fig. 3*C*). Because RhoC was not expressed in these cells (Fig. 3*C*), RhoA/RhoB dKO macrophages were deficient in all three Rho isoforms. When compared with unstimulated WT cells, unstimulated macrophages from RhoB$^{-/-}$ mice typically exhibited a rounded morphology, characterized by a paucity of lamellipodial extensions (Fig. 3*D*). To confirm that the rounded up RhoB$^{-/-}$ cells were macrophages, we incubated living cells with anti-F4/80 antibodies conjugated to Alexa Fluor 488 (F4/80 is a mouse macrophage marker). The rounded up morphology of RhoB$^{-/-}$ cells can probably be explained by increased RhoA levels (Fig. 3, *A* and *B*). When wild-type and RhoB$^{-/-}$ macrophages were activated with the Toll-like receptor 4 ligand LPS, the cells spread out and assumed a morphology similar to wild-type cells (Fig. 3*D*). Strikingly, RhoA/RhoB dKO macrophages exhibited highly elongated and branched morphologies. This phenotype was more pronounced in cells stimulated with LPS (Fig. 3*D*), which promotes increased lamellipodial membrane dynamics and random motility.

The extremely aberrant morphologies of RhoA/RhoB dKO macrophages, when compared with RhoA$^{-/-}$ or RhoB$^{-/-}$ cells, underscore that RhoA and RhoB are capable of mutual functional compensation. High resolution images of fixed WT and RhoA/RhoB dKO macrophages, obtained by superresolution structured illumination microscopy, revealed a dense meshwork of secondary F-actin structures, but a paucity of actin stress fibers, in both cell types (Fig. 3*E*).

In time-lapse DIC recordings, we observed the development of multiple branches in randomly migrating RhoA/RhoB dKO macrophages (Fig. 4*A*). The mean numbers of primary branches in randomly migrating wild-type, RhoB$^{-/-}$, and RhoA/RhoB dKO macrophages are shown in Fig. 4*B*. Branches arose from the incomplete retraction of trailing ends and lamellipodia, as shown in Fig. 4, *A* and *C* (see also supplemental Video 1). Macrophages lacking the Rho subfamily also exhibited erratic multifocal membrane protrusions, which were most evident in cells lacking a large dominant lamellipodium (Fig. 4*D*).

Robust Motility and Chemotaxis of Pan-Rho Knock-out (RhoA$^{fl/fl}$/LysM-Cre/RhoB$^{-/-}$) Macrophages—Migration plots of RhoB$^{-/-}$ and RhoA/RhoB dKO macrophages are shown in Fig. 5*A*. RhoB$^{-/-}$ macrophages had impaired chemotactic efficiency, but normal velocity, when compared with wild-type cells (Fig. 5*B*). Surprisingly, the chemotactic efficiency of RhoA/RhoB dKO macrophages was not impaired, but these cells had a significantly higher mean velocity than wild-type cells (Fig. 5*B*). Note that we routinely tracked the cell body, except, in the case of RhoA/RhoB dKO macrophages, we additionally tracked the trailing end (Fig. 5*B*). Snapshots of RhoB$^{-/-}$ and RhoA/RhoB dKO macrophages migrating in a chemotactic C5a gradient are shown in Fig. 5*C* (see also time-lapse movies, supplemental Videos 2 and 3). RhoA/RhoB dKO macrophages migrating toward a chemoattractant source developed exceedingly long (frequently >200-μm) trailing ends. We measured the maximal tail length developed by macrophages migrating in a chemotactic gradient over a 6-h period (Fig. 5*D*). Tails lengths were much greater in RhoA/RhoB dKO macrophages than in RhoA$^{-/-}$ (RhoA$^{fl/fl}$/LysM-Cre) or RhoB$^{-/-}$ cells, implying that both RhoA and RhoB are involved in tail retraction or, at least, each can mutually compensate deficiency of the other. Although the trailing edge was often lagging far behind in migrating dKO cells, it would, at some point, spring back toward the cell body, analogous to the sudden release of an elastic thread. We presume that this effect was due to reaction forces caused by forward translocation of the cell body (37). To investigate whether lack of myosin II light chain phosphorylation in RhoA/RhoB dKO macrophages may contribute to impaired lamellipodial and tail retraction, we analyzed phospho-myosin light chain 2 (p-MLC2) levels by Western blot (Fig. 5*E*). Surprisingly, p-MLC2 levels were increased by a factor of 3.3 ± 0.5 ($n = 3$) in RhoA/RhoB dKO macrophages, when compared with WT cells.

In Vivo Peritonitis Model—We tested whether the tail and lamellipodial retraction defects observed *in vitro* translated *in vivo* to impaired recruitment of RhoA/RhoB-deficient cells (Fig. 5*F*). On the contrary, we found in a mouse model of thioglycollate-mediated peritonitis that F4/80-positive cells (monocytes and macrophages) were recruited more rapidly

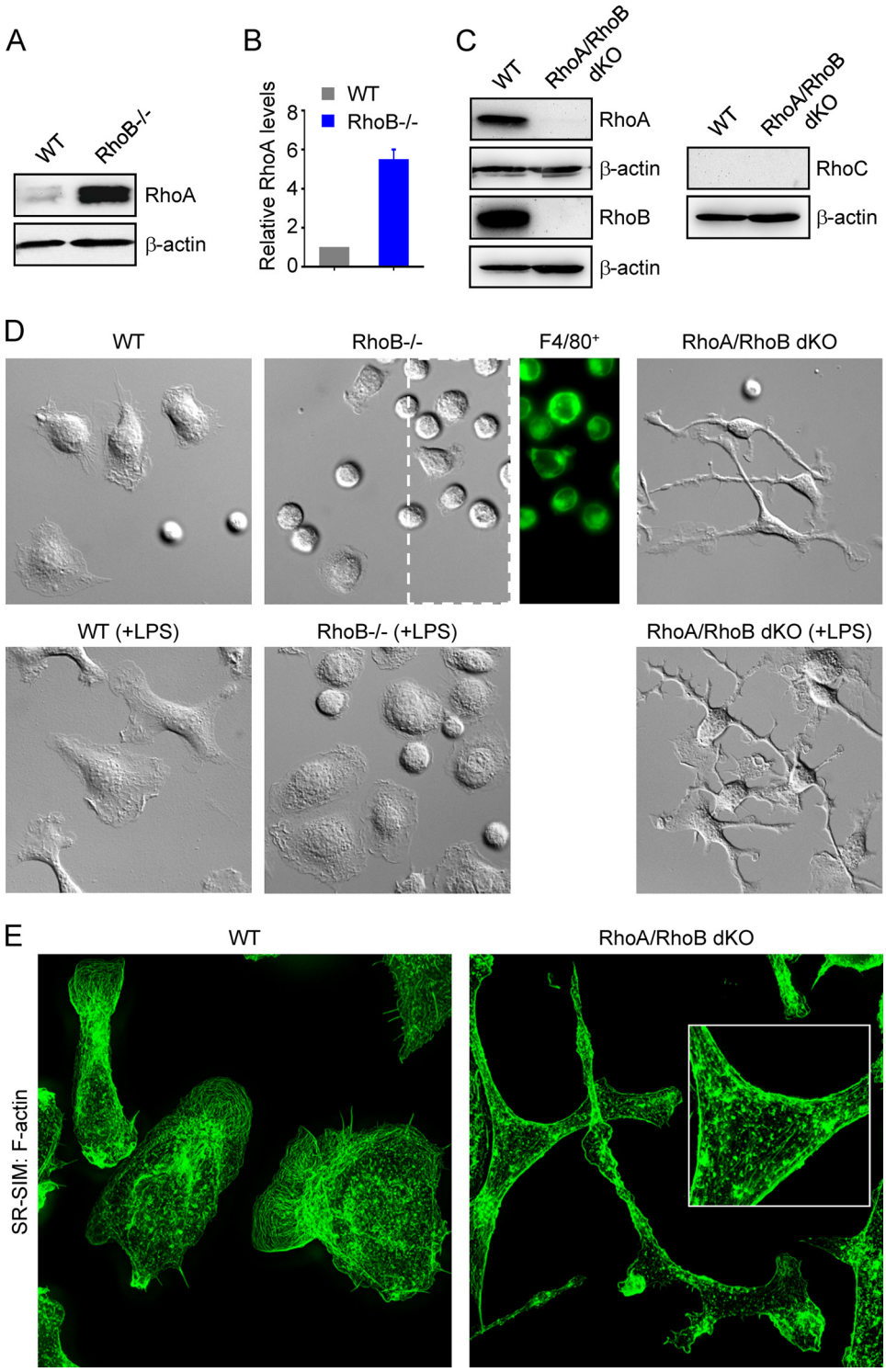

FIGURE 3. **Striking phenotype and chemotactic behavior of pan-Rho-deficient (RhoA$^{fl/fl}$/LysM-Cre/RhoB$^{-/-}$) macrophages.** *A*, Western blot analysis of RhoA in macrophages derived from WT and RhoB$^{-/-}$ mice. *B*, high expression levels of RhoA in RhoB$^{-/-}$ macrophages relative to wild-type cells ($n = 3$). *Error bars* indicate means ± S.E. *C*, Western blot analysis of RhoA, RhoB, and RhoC in macrophages derived from WT and RhoA/RhoB dKO (double knock-out; RhoA$^{fl/fl}$/LysM-Cre/RhoB$^{-/-}$) mice. *D*, morphology of WT, RhoB$^{-/-}$ and RhoA/RhoB dKO macrophages under conditions of no stimulation (*upper panel*) or activation (*lower panel*) with 100 ng/ml lipopolysaccharide (+*LPS*). The DIC images are 100 × 100 μm. F4/80 staining (*green*) was used to confirm that the unstimulated and rounded up RhoB$^{-/-}$ cells shown are macrophages. *E*, superresolution structured illumination microscopy (*SR-SIM*) images of fixed WT and RhoA/RhoB dKO macrophages. F-actin was labeled using Alexa Fluor 488-conjugated phalloidin. The *inset* (*right image*) provides an enlarged view of the actin cytoskeleton.

to the peritoneal cavity in myeloid-restricted RhoA/RhoB dKO mice than in RhoA$^{fl/fl}$ mice, used as control (Fig. 5*F*). Thus, Rho signaling in mononuclear phagocytes is not essential to overcome physiological barriers imposed by the endothelium, basement membrane, and interstitial matrix in the peritoneum.

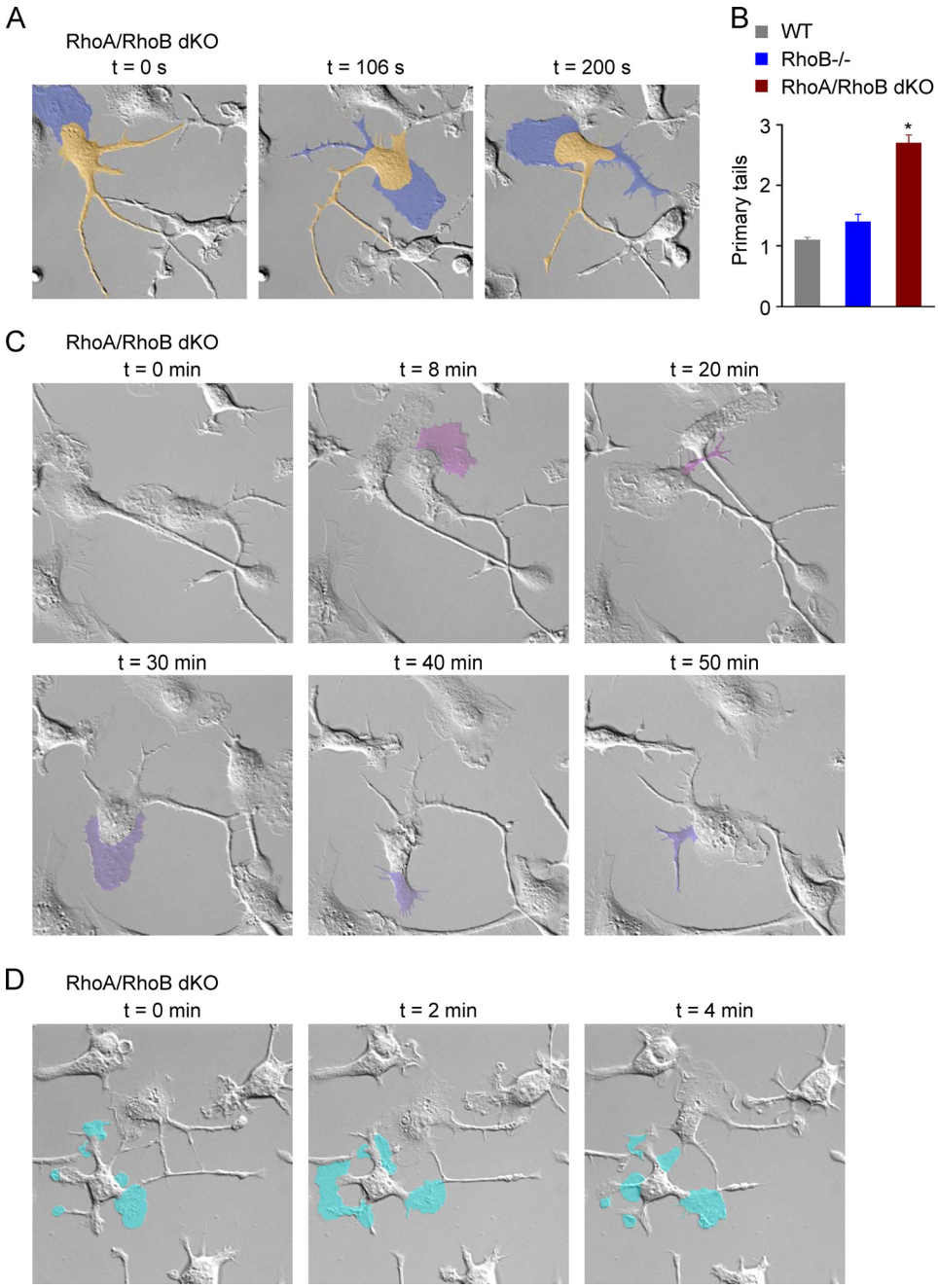

FIGURE 4. **Mechanism of branch formation in spontaneously migrating pan-Rho-deficient (RhoA$^{fl/fl}$/LysM-Cre/RhoB$^{-/-}$) macrophages.** *A*, time-lapse DIC images (100 × 100 μm) of a spontaneously migrating RhoA/RhoB dKO (RhoA$^{fl/fl}$/LysM-Cre/RhoB$^{-/-}$) macrophage. The dominant lamellipodium, as well as its remnants after incomplete retraction and relocation, have been pseudocolored *blue*. The rest of the cell has been pseudocolored *pale brown* (*beige*). *B*, mean number of primary branches arising from the cell body of WT, RhoB$^{-/-}$, and RhoA/RhoB dKO macrophages. *, $p < 0.05$ (Kruskal-Wallis test and post hoc Dunn test). *Error bars* indicate means ± S.E. *C*, further examples of branch formation arising from incomplete membrane retraction following relocation of the dominant lamellipodium. Note that when the lamellipodium (pseudocolored) shifts location, it leaves behind a branch (correspondingly pseudocolored). The DIC images are 100 × 100 μm. *D*, time-lapse DIC images (100 × 100 μm) showing erratic multifocal membrane protrusions (pseudocolored *light blue*) in a RhoA/RhoB dKO macrophage.

Deletion of RhoB Partially Rescues the Motility Defect of Myo9b$^{-/-}$ Macrophages—The motorized RhoGAP Myo9b is a key negative regulator of Rho in leukocytes (1, 38). We next tested whether genetic deletion of RhoB rescued the motility defect of macrophages lacking Myo9b (1). Spinning disk confocal microscopy of fluorescently labeled macrophages seeded into fibronectin coated Ibidi μ-slide I chambers showed that, similar to Myo9b$^{-/-}$ macrophages (1), Myo9b/RhoB dKO cells exhibit an aberrant rounded morphology (Fig. 6*A*). Active RhoA (RhoA-GTP) levels, but not total RhoA, are known to be increased in mouse macrophages (1) and dendritic cells (38). We found that total RhoB levels were markedly reduced in Myo9b$^{-/-}$ macrophages, when compared with WT cells (Fig. 6, *B* and *C*). We next tested whether deletion of RhoB partially rescues motility in Myo9b$^{-/-}$ mice. Indeed, this was the case (Fig. 7). Phase-contrast snapshots of cells in a C5a gradient showed that both Myo9b$^{-/-}$ and Myo9b/RhoB dKO cells migrated with an aberrant compact morphology (Fig. 7*A*).

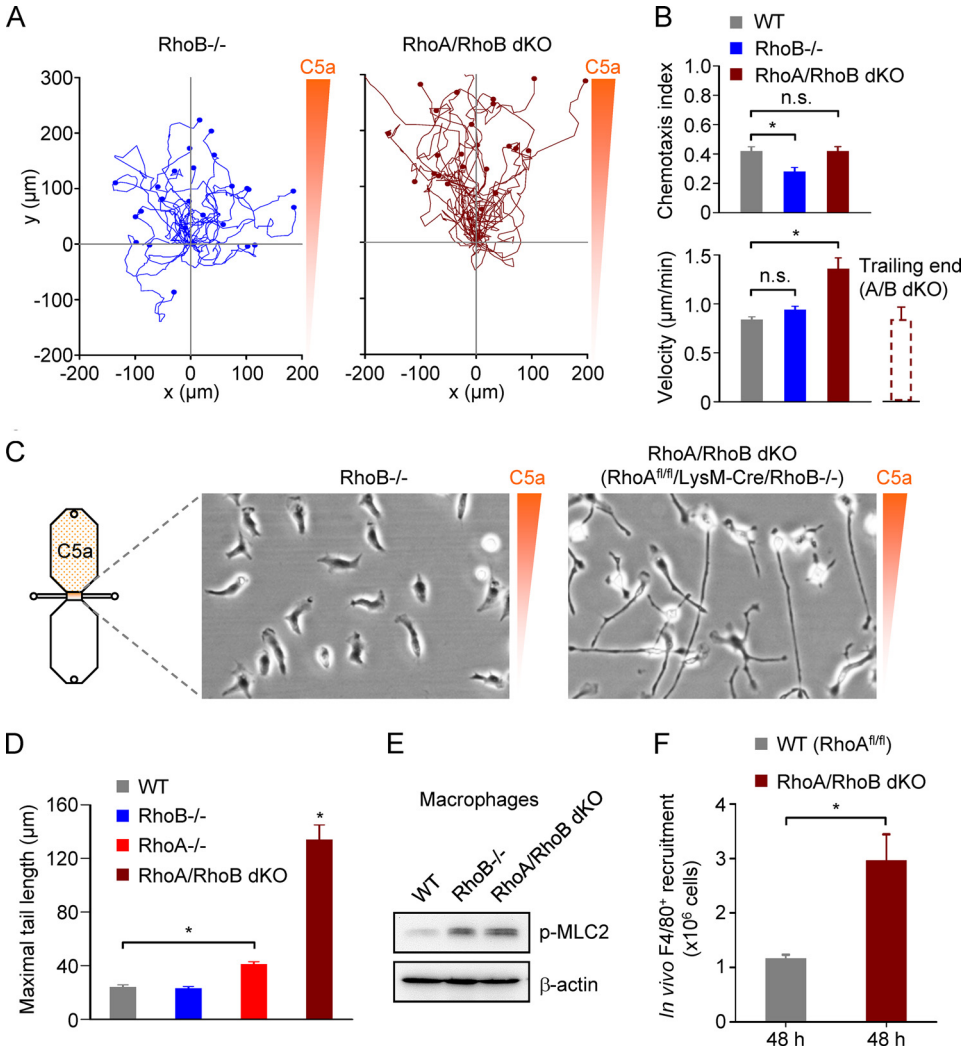

FIGURE 5. **Pan-Rho-deficient (RhoA$^{fl/fl}$/LysM-Cre/RhoB$^{-/-}$) macrophages develop exceedingly long trailing ends during chemotaxis.** *A*, migration plots of RhoB$^{-/-}$ and RhoA/RhoB dKO macrophages in a complement component C5a gradient. *B*, summary plots of chemotactic efficiency (chemotaxis index) and mean velocity, comparing WT, RhoB$^{-/-}$, and RhoA/RhoB dKO (double knock-out; RhoA$^{fl/fl}$/LysM-Cre/RhoB$^{-/-}$) macrophages. Data were obtained after tracking the cell body, except in the fourth column (*lower plot*), which shows mean velocity of the trailing end of RhoA/RhoB (*A/B*) dKO macrophages. *C*, schematic diagram of a chemotaxis slide and 200 × 300-μm snapshots of RhoB$^{-/-}$ and RhoA/RhoB dKO macrophages in a chemotactic C5a gradient. *D*, plot of maximal tail length observed in WT, RhoB$^{-/-}$, RhoA$^{fl/fl}$/LysM-Cre (RhoA$^{-/-}$), and RhoA/RhoB dKO macrophages migrating in a chemotactic gradient during a 6-h period. *E*, Western blot analysis of p-MLC2 levels in WT, RhoB$^{-/-}$, and RhoA/RhoB dKO macrophages. *F*, plot of the total number of F4/80^{+} cells that accumulated in the peritoneal cavity of WT (RhoA$^{fl/fl}$) and RhoA/RhoB dKO mice 48 h after intraperitoneal injection of thioglycollate. *, $p < 0.05$ (Kruskal-Wallis test and post hoc Dunn test or, in the case of *panel F*, unpaired Student's *t* test). *n.s.*, not significant. *Error bars* indicate means ± S.E.

When compared with Myo9b$^{-/-}$ cells, motility was partially rescued in Myo9b/RhoB dKO macrophages (Fig. 7, *B* and *C*).

DISCUSSION

One of the key elements of current models of cell motility and chemotaxis is RhoA, a member of the Rho subfamily of GTPases, which includes RhoB and RhoC. In this study, we used knock-out mouse models and real-time imaging to analyze systematically the roles of the Rho subfamily of GTPases and the RhoGAP Myo9b in macrophage cell shape control, motility, and chemotactic navigation. As a starting point, we found that loss of RhoA was associated with moderately impaired tail retraction, as expected from the literature (2, 39), but velocity and chemotactic navigation were unaffected. Loss of RhoB was not associated with impaired tail retraction, and velocity was unaffected. However, RhoB-deficient macrophages exhibited a paucity of lamellipodial membrane protrusions, giving rise to a rounded up morphology, which could be reversed by stimulating cells with the Toll-like receptor 4 ligand LPS. Moreover, chemotactic efficiency was impaired in RhoB-deficient macrophages. Notably, RhoB levels were markedly increased in RhoA-deficient macrophages, and conversely, RhoA levels were increased in RhoB$^{-/-}$ macrophages. These observations suggested that the highly homologous proteins RhoA and RhoB (located on chromosomes 9 and 12, respectively) may mutually compensate the loss of either isoform. Indeed, genetic deletion of both RhoA and RhoB did not evoke RhoC expression, and double mutant macrophages developed overtly aberrant phenotypes.

RhoA/RhoB dKO macrophages, which lack the entire Rho subfamily of RhoGTPases, were observed migrating in a chemotactic gradient and randomly at high resolution. Surpris-

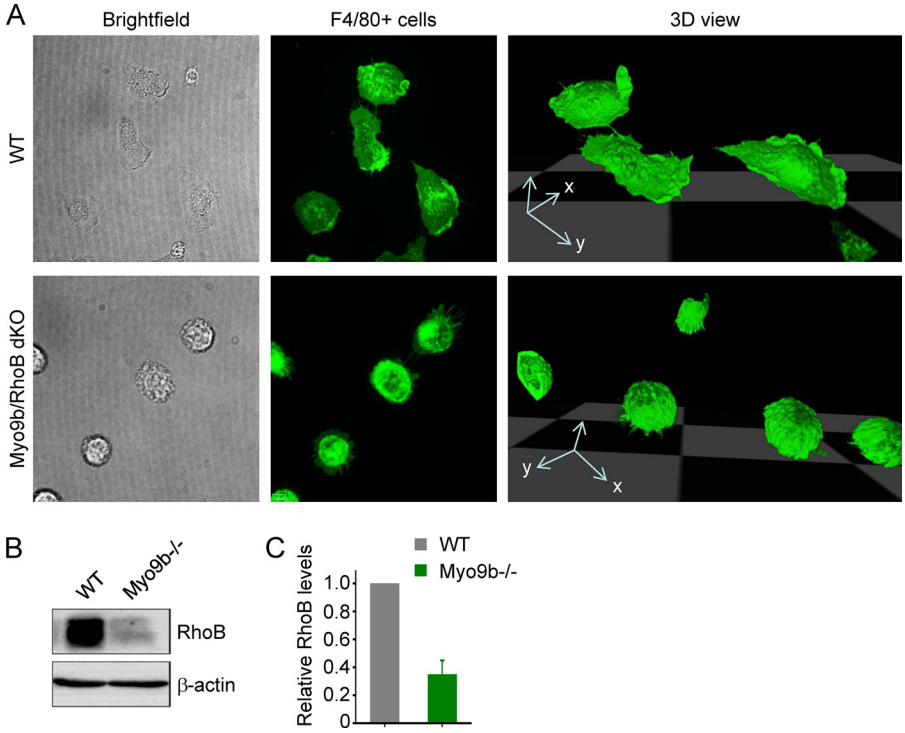

FIGURE 6. **Phenotype of Myo9b/RhoB double knock-out macrophages.** *A*, bright-field and extended focus images (120 × 120 μm) of living WT and Myo9b/RhoB dKO macrophages, labeled with Alexa Fluor 488-conjugated anti-F4/80 antibodies and imaged by spinning disk confocal microscopy. Three-dimensional views of the same cells are shown on the *right*. *B*, Western blot analysis of RhoB in macrophages derived from WT and Myo9b$^{-/-}$ mice. *C*, low expression levels of RhoB in Myo9b$^{-/-}$ macrophages relative to WT cells ($n = 3$). *Error bars* indicate means ± S.E.

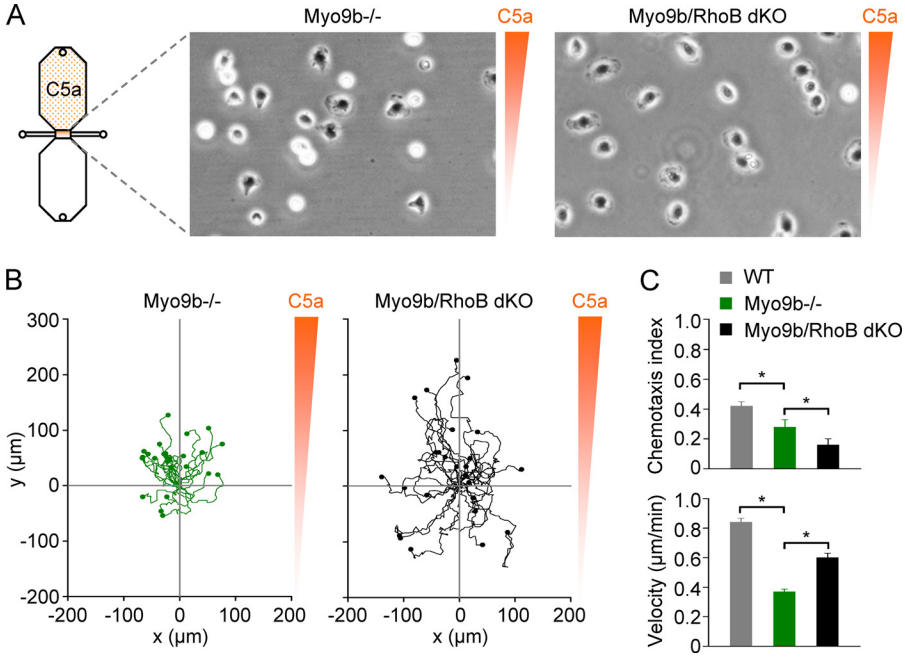

FIGURE 7. **Genetic deletion of RhoB in Myo9b$^{-/-}$ macrophages partially rescues velocity.** *A*, schematic diagram of a chemotaxis μ-slide and 200 × 300-μm snapshots of Myo9b$^{-/-}$ and Myo9b/RhoB dKO macrophages in a chemotactic complement component C5a gradient. *B*, migration plots of Myo9b$^{-/-}$ and Myo9b/RhoB dKO macrophages in a C5a gradient. *C*, summary plots of chemotactic efficiency (chemotaxis index) and mean velocity, comparing WT, Myo9b$^{-/-}$, and Myo9b/RhoB dKO macrophages. *, $p < 0.05$ (Kruskal-Wallis test and post hoc Dunn test). *Error bars* indicate means ± S.E.

ingly, the cell body of RhoA/RhoB dKO mutants was faster than WT controls and chemotactic efficiency was not impaired, but the trailing end became extremely elongated, frequently exceeding 200 μm in length. This extreme phenotype was absent in RhoB$^{-/-}$ macrophages, and in RhoA-deficient cells, tail elongation was compensated by more than 80%, underscoring that RhoA and RhoB mutually compensate loss of function. We infer that both RhoA and RhoB are involved in tail retraction, but RhoA is predominant, possibly due to the shorter half-life of RhoB in the plasma membrane (40). The tail retraction

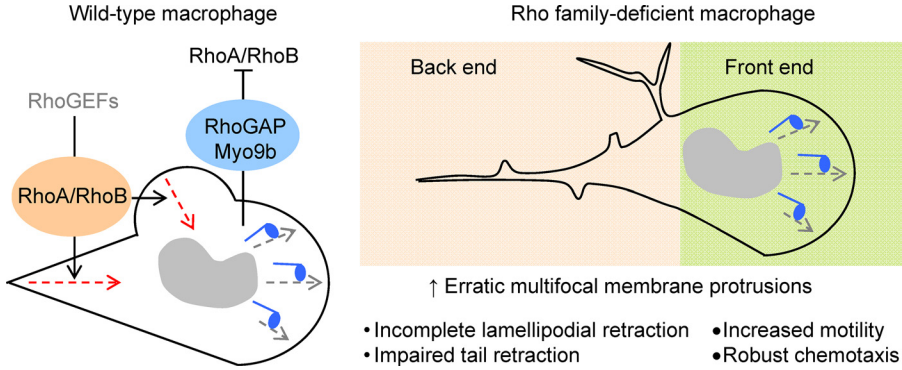

FIGURE 8. **Schematic diagrams indicating the roles of Rho proteins and the negative regulator Myo9b in directed macrophage motility.** In wild-type macrophages, both active RhoA and RhoB are involved in the retraction (*red arrows*) of the trailing end and membrane protrusions, whereas the RhoGAP Myo9b acts at the front to inactivate both RhoA and RhoB. In the absence of the Rho subfamily, there is severely impaired lamellipodial membrane and tail retraction at the back end, but increased motility and robust chemotaxis of the front end (cell body). In addition, macrophages lacking the Rho subfamily exhibit erratic multifocal membrane protrusions.

defect was presumably due to loss of Rho-ROCK-myosin II signaling in RhoA/RhoB double knock-out mutants. Inhibition of ROCK (1) or myosin II[3] produces the same defect. However, we found that phospho-myosin light chain 2 levels were increased in RhoA/RhoB dKO, when compared with WT, macrophages, suggesting that alternative pathways to Rho-ROCK signaling are more active in dKO cells, such as myosin light chain kinase or myotonic dystrophy kinase-related Cdc42-binding kinase (41). Typically, the exceedingly long tail of migrating pan-Rho-deficient macrophages would spring back toward the cell body, presumably when the front end generated sufficient reaction force to disrupt cell-substrate adhesions at the back. Calcium/calmodulin signaling, implicated in the tail retraction of migrating neutrophils (42) and fibroblasts (43), may also contribute to myosin II activation in the absence of Rho signaling.

Aside from the phenotype of elongated trailing ends, RhoA/RhoB double knock-out macrophages exhibited severely impaired retraction of lamellipodial membrane protrusions during spontaneous cell migration, which gave rise to highly ramified cell morphologies. Analysis of time-lapse DIC images revealed that branches can arise when macrophages change the direction of movement. Unlike some cells, such as neutrophils, which make U-turns to change direction (44, 45), macrophages can change direction by splitting or reorienting a dominant lamellipodium or by moving the lamellipodium across the cell body in a remarkably fluid fashion. However, in macrophages lacking Rho, the "old" lamellipodium is not completely resorbed into the cell body, leaving behind prominent branches and membranous streaks.

In addition to severely impaired tail retraction and the formation of prominent branches, a third phenotypic feature of RhoA/RhoB dKO macrophages was the appearance of erratic multifocal membrane protrusions, especially in stationary cells lacking a clear dominant lamellipodium. We did not investigate this observation in detail, although it fits in with the notions that both active Rho and membrane tension produced by leading edge protrusion act to suppress multifocal membrane protrusions (19, 46). Aside from motility, the Rho subfamily has been implicated in endosomal trafficking (18) and the "sink in" mode of phagocytosis (47), a fundamental function of professional phagocytes. In future studies, it would be interesting to explore whether complement receptor-mediated phagocytosis is impaired in RhoA/RhoB dKO macrophages.

The physiological consequences of macrophage pan-Rho deficiency in terms of *in vivo* cell recruitment are difficult to predict. On the one hand, we found that RhoA/RhoB dKO macrophages migrate more rapidly than wild-type cells *in vitro*, whereas on the other hand, Rho-ROCK signaling has been implicated in the squeezing of leukocytes through narrow pores in three-dimensional environments (20). It was therefore somewhat surprising that RhoA/RhoB dKO monocytes and macrophages were recruited more rapidly than WT cells in an *in vivo* peritonitis model. This finding indicates that the Rho subfamily is not required for monocytes to egress through a continuous endothelium, at least in the peritoneum. Gautier *et al.* (48) showed that the clearance of macrophages from thioglycollate-induced peritonitis is mediated principally via macrophage apoptosis rather than emigration to lymph nodes, as previously thought (49). Thus, we would expect that the clearance of macrophages during the resolution phase of peritoneal inflammation, in which emigration to draining lymph nodes plays a minor role, would not be significantly affected in myeloid-restricted RhoA/RhoB dKO mice.

An important negative regulator of the Rho subfamily in macrophages is the RhoGAP Myo9b. We have previously reported that macrophages isolated from mice lacking Myo9b have an aberrant round morphology, associated with increased RhoA activity, as well as decreased motility and impaired chemotaxis (1). We extended this work and found that, when compared with WT cells, RhoB levels are decreased in Myo9b$^{-/-}$ macrophages, although we did not measure active RhoB levels. Genetic deletion of RhoB in Myo9b$^{-/-}$ macrophages did not abrogate the rounded up phenotype, but motility was partially rescued. Because the nonselective Rho inhibitor TAT-C3 rescues the rounded up phenotype (1), we infer that genetic deletion of RhoA or, possibly, both RhoA and RhoB, is required to re-establish morphological cell polarization in Myo9b$^{-/-}$ macrophages.

[3] V. Königs, R. Jennings, T. Vogl, M. Horsthemke, A. C. Bachg, Y. Xu, K. Grobe, C. Brakebusch, A. Schwab, M. Bähler, U. G. Knaus, and P. J. Hanley, unpublished observations.

In summary, our data suggest a model (see Fig. 8) in which both active RhoA and RhoB are involved in back end functions, such as retracting the tail and lamellipodial membrane extensions, whereas the RhoGAP Myo9b ensures inactivation of both RhoA and RhoB at the front end. In the absence of the Rho subfamily, Myo9b is redundant, and *in vitro* and *in vivo* data indicate that front end (cell body) functions, such as motility and chemotactic navigation, are not critically dependent on Rho.

Note Added in Proof—Dashed vertical lines were added to Fig. 1*D* to indicate where the images were spliced together.

REFERENCES

1. Hanley, P. J., Xu, Y., Kronlage, M., Grobe, K., Schön, P., Song, J., Sorokin, L., Schwab, A., and Bähler, M. (2010) Motorized RhoGAP myosin IXb (Myo9b) controls cell shape and motility. *Proc. Natl. Acad. Sci. U.S.A.* **107,** 12145–12150
2. Ridley, A. J., Schwartz, M. A., Burridge, K., Firtel, R. A., Ginsberg, M. H., Borisy, G., Parsons, J. T., and Horwitz, A. R. (2003) Cell migration: integrating signals from front to back. *Science* **302,** 1704–1709
3. Abercrombie, M., Heaysman, J. E., and Pegrum, S. M. (1971) The locomotion of fibroblasts in culture. IV. Electron microscopy of the leading lamella. *Exp. Cell Res.* **67,** 359–367
4. Reig, G., Pulgar, E., and Concha, M. L. (2014) Cell migration: from tissue culture to embryos. *Development* **141,** 1999–2013
5. Swaney, K. F., Huang, C. H., and Devreotes, P. N. (2010) Eukaryotic chemotaxis: a network of signaling pathways controls motility, directional sensing, and polarity. *Annu. Rev. Biophys.* **39,** 265–289
6. Huang, C. H., Tang, M., Shi, C., Iglesias, P. A., and Devreotes, P. N. (2013) An excitable signal integrator couples to an idling cytoskeletal oscillator to drive cell migration. *Nat. Cell Biol.* **15,** 1307–1316
7. Wennerberg, K., and Der, C. J. (2004) Rho-family GTPases: it's not only Rac and Rho (and I like it). *J. Cell Sci.* **117,** 1301–1312
8. Tybulewicz, V. L., and Henderson, R. B. (2009) Rho family GTPases and their regulators in lymphocytes. *Nat. Rev. Immunol.* **9,** 630–644
9. Rougerie, P., and Delon, J. (2012) Rho GTPases: Masters of T lymphocyte migration and activation. *Immunol. Lett.* **142,** 1–13
10. Schwab, A., Fabian, A., Hanley, P. J., and Stock, C. (2012) Role of ion channels and transporters in cell migration. *Physiol. Rev.* **92,** 1865–1913
11. Pollard, T. D., and Borisy, G. G. (2003) Cellular motility driven by assembly and disassembly of actin filaments. *Cell* **112,** 453–465
12. Tyska, M. J., Dupuis, D. E., Guilford, W. H., Patlak, J. B., Waller, G. S., Trybus, K. M., Warshaw, D. M., and Lowey, S. (1999) Two heads of myosin are better than one for generating force and motion. *Proc. Natl. Acad. Sci. U.S.A.* **96,** 4402–4407
13. Footer, M. J., Kerssemakers, J. W., Theriot, J. A., and Dogterom, M. (2007) Direct measurement of force generation by actin filament polymerization using an optical trap. *Proc. Natl. Acad. Sci. U.S.A.* **104,** 2181–2186
14. Rose, R., Weyand, M., Lammers, M., Ishizaki, T., Ahmadian, M. R., and Wittinghofer, A. (2005) Structural and mechanistic insights into the interaction between Rho and mammalian Dia. *Nature* **435,** 513–518
15. Goh, W. I., and Ahmed, S. (2012) mDia1–3 in mammalian filopodia. *Commun. Integr. Biol.* **5,** 340–344
16. Lammers, M., Meyer, S., Kühlmann, D., and Wittinghofer, A. (2008) Specificity of interactions between mDia isoforms and Rho proteins. *J. Biol. Chem.* **283,** 35236–35246
17. Kaibuchi, K., Kuroda, S., and Amano, M. (1999) Regulation of the cytoskeleton and cell adhesion by the Rho family GTPases in mammalian cells. *Annu. Rev. Biochem.* **68,** 459–486
18. Wheeler, A. P., and Ridley, A. J. (2004) Why three Rho proteins? RhoA, RhoB, RhoC, and cell motility. *Exp. Cell Res.* **301,** 43–49
19. Worthylake, R. A., and Burridge, K. (2003) RhoA and ROCK promote migration by limiting membrane protrusions. *J. Biol. Chem.* **278,** 13578–13584
20. Lämmermann, T., Bader, B. L., Monkley, S. J., Worbs, T., Wedlich-Söldner, R., Hirsch, K., Keller, M., Förster, R., Critchley, D. R., Fässler, R., and Sixt, M. (2008) Rapid leukocyte migration by integrin-independent flowing and squeezing. *Nature* **453,** 51–55
21. Pertz, O., Hodgson, L., Klemke, R. L., and Hahn, K. M. (2006) Spatiotemporal dynamics of RhoA activity in migrating cells. *Nature* **440,** 1069–1072
22. Machacek, M., Hodgson, L., Welch, C., Elliott, H., Pertz, O., Nalbant, P., Abell, A., Johnson, G. L., Hahn, K. M., and Danuser, G. (2009) Coordination of Rho GTPase activities during cell protrusion. *Nature* **461,** 99–103
23. Wettschureck, N., and Offermanns, S. (2005) Mammalian G proteins and their cell type specific functions. *Physiol. Rev.* **85,** 1159–1204
24. Worzfeld, T., Wettschureck, N., and Offermanns, S. (2008) G_{12}/G_{13}-mediated signalling in mammalian physiology and disease. *Trends Pharmacol. Sci.* **29,** 582–589
25. Kozasa, T., Hajicek, N., Chow, C. R., and Suzuki, N. (2011) Signalling mechanisms of RhoGTPase regulation by the heterotrimeric G proteins G12 and G13. *J. Biochem.* **150,** 357–369
26. Vogt, S., Grosse, R., Schultz, G., and Offermanns, S. (2003) Receptor-dependent RhoA activation in G_{12}/G_{13}-deficient cells: genetic evidence for an involvement of G_q/G_{11}. *J. Biol. Chem.* **278,** 28743–28749
27. Lutz, S., Freichel-Blomquist, A., Yang, Y., Rümenapp, U., Jakobs, K. H., Schmidt, M., and Wieland, T. (2005) The guanine nucleotide exchange factor p63RhoGEF, a specific link between $G_{q/11}$-coupled receptor signaling and RhoA. *J. Biol. Chem.* **280,** 11134–11139
28. Liu, A. X., Rane, N., Liu, J. P., and Prendergast, G. C. (2001) RhoB is dispensable for mouse development, but it modifies susceptibility to tumor formation as well as cell adhesion and growth factor signaling in transformed cells. *Mol. Cell. Biol.* **21,** 6906–6912
29. Hakem, A., Sanchez-Sweatman, O., You-Ten, A., Duncan, G., Wakeham, A., Khokha, R., and Mak, T. W. (2005) RhoC is dispensable for embryogenesis and tumor initiation but essential for metastasis. *Genes Dev.* **19,** 1974–1979
30. Wheeler, A. P., and Ridley, A. J. (2007) RhoB affects macrophage adhesion, integrin expression and migration. *Exp. Cell Res.* **313,** 3505–3516
31. Ridley, A. J. (2013) RhoA, RhoB and RhoC have different roles in cancer cell migration. *J. Microsc.* **251,** 242–249
32. Thumkeo, D., Watanabe, S., and Narumiya, S. (2013) Physiological roles of Rho and Rho effectors in mammals. *Eur. J. Cell Biol.* **92,** 303–315
33. Melendez, J., Stengel, K., Zhou, X., Chauhan, B. K., Debidda, M., Andreassen, P., Lang, R. A., and Zheng, Y. (2011) RhoA GTPase is dispensable for actomyosin regulation but is essential for mitosis in primary mouse embryonic fibroblasts. *J. Biol. Chem.* **286,** 15132–15137
34. Jackson, B., Peyrollier, K., Pedersen, E., Basse, A., Karlsson, R., Wang, Z., Lefever, T., Ochsenbein, A. M., Schmidt, G., Aktories, K., Stanley, A., Quondamatteo, F., Ladwein, M., Rottner, K., van Hengel, J., and Brakebusch, C. (2011) RhoA is dispensable for skin development, but crucial for contraction and directed migration of keratinocytes. *Mol. Biol. Cell* **22,** 593–605
35. Clausen, B. E., Burkhardt, C., Reith, W., Renkawitz, R., and Förster, I. (1999) Conditional gene targeting in macrophages and granulocytes using LysMcre mice. *Transgenic Res.* **8,** 265–277
36. Faust, N., Varas, F., Kelly, L. M., Heck, S., and Graf, T. (2000) Insertion of enhanced green fluorescent protein into the lysozyme gene creates mice with green fluorescent granulocytes and macrophages. *Blood* **96,** 719–726
37. Pathak, A., and Kumar, S. (2011) From molecular signal activation to locomotion: an integrated, multiscale analysis of cell motility on defined matrices. *PLoS One* **6,** e18423
38. Xu, Y., Pektor, S., Balkow, S., Hemkemeyer, S. A., Liu, Z., Grobe, K., Hanley, P. J., Shen, L., Bros, M., Schmidt, T., Bähler, M., and Grabbe, S. (2014) Dendritic cell motility and T cell activation requires regulation of Rho-cofilin signaling by the Rho-GTPase activating protein myosin IXb. *J. Immunol.* **192,** 3559–3568
39. Pestonjamasp, K. N., Forster, C., Sun, C., Gardiner, E. M., Bohl, B., Weiner, O., Bokoch, G. M., and Glogauer, M. (2006) Rac1 links leading edge and uropod events through Rho and myosin activation during chemotaxis. *Blood* **108,** 2814–2820
40. Pérez-Sala, D., Boya, P., Ramos, I., Herrera, M., and Stamatakis, K. (2009) The C-terminal sequence of RhoB directs protein degradation through an

endo-lysosomal pathway. *PLoS One* **4,** e8117
41. Wilkinson, S., Paterson, H. F., and Marshall, C. J. (2005) Cdc42-MRCK and Rho-ROCK signalling cooperate in myosin phosphorylation and cell invasion. *Nat. Cell Biol.* **7,** 255–261
42. Eddy, R. J., Pierini, L. M., Matsumura, F., and Maxfield, F. R. (2000) Ca^{2+}-dependent myosin II activation is required for uropod retraction during neutrophil migration. *J. Cell Sci.* **113,** 1287–1298
43. Yang, S., and Huang, X. Y. (2005) Ca^{2+} influx through L-type Ca^{2+} channels controls the trailing tail contraction in growth factor-induced fibroblast cell migration. *J. Biol. Chem.* **280,** 27130–27137
44. Xu, J., Wang, F., Van Keymeulen, A., Herzmark, P., Straight, A., Kelly, K., Takuwa, Y., Sugimoto, N., Mitchison, T., and Bourne, H. R. (2003) Divergent signals and cytoskeletal assemblies regulate self-organizing polarity in neutrophils. *Cell* **114,** 201–214
45. Zigmond, S. H., Levitsky, H. I., and Kreel, B. J. (1981) Cell polarity: an examination of its behavioral expression and its consequences for polymorphonuclear leukocyte chemotaxis. *J. Cell Biol.* **89,** 585–592
46. Houk, A. R., Jilkine, A., Mejean, C. O., Boltyanskiy, R., Dufresne, E. R., Angenent, S. B., Altschuler, S. J., Wu, L. F., and Weiner, O. D. (2012) Membrane tension maintains cell polarity by confining signals to the leading edge during neutrophil migration. *Cell* **148,** 175–188
47. Chimini, G., and Chavrier, P. (2000) Function of Rho family proteins in actin dynamics during phagocytosis and engulfment. *Nat. Cell Biol.* **2,** E191–E196
48. Gautier, E. L., Ivanov, S., Lesnik, P., and Randolph, G. J. (2013) Local apoptosis mediates clearance of macrophages from resolving inflammation in mice. *Blood* **122,** 2714–2722
49. Bellingan, G. J., Caldwell, H., Howie, S. E., Dransfield, I., and Haslett, C. (1996) *In vivo* fate of the inflammatory macrophage during the resolution of inflammation: inflammatory macrophages do not die locally, but emigrate to the draining lymph nodes. *J. Immunol.* **157,** 2577–2585